Rejecting Impulse Artifacts from Surface EMG Signals using Real-time Cumulative Histogram Filtering

Seong Ho Yeon[1] and Hugh M. Herr[1]

Abstract— This paper presents a cumulative histogram filtering (CHF) algorithm to filter impulsive artifacts within surface electromyograhy (sEMG) signal for time-domain signal feature extraction. The proposed CHF algorithm filters sEMG signals by extracting a continuous subset of amplitude-sorted values within a real-time window of measured samples using information about the probabilistic distribution of sEMG amplitude. For real-time deployment of the proposed CHF algorithm on an embedded computing platform, we also present an efficient, iterative implementation of the proposed algorithm. The proposed CHF algorithm was evaluated on synthetic impulse artifacts superimposed upon undisturbed sEMG recorded from a subject with transtibial amputation. Results suggest that the CHF algorithm effectively suppresses the simulated impulse artifacts while preserving a minimum signal-to-noise ratio of 95% and an average Pearson correlation of 0.99 compared to the undisturbed sEMG recordings.

I. INTRODUCTION

The study of surface electromyography (sEMG) over the past couple of decades has enabled varied applications of neural control in upper and lower extremity prosthetic devices [1]. Due to the non-stationary and chaotic nature of sEMG signals, numerous attempts have been made to understand and interpret sEMG signals in meaningful, physiological terms related to collective muscle unit action potentials (MUAPs), muscle state, muscle force, muscle synergies, and even the kinematics and kinetics of muscle [1]–[6]. Among these studies, early seminal results demonstrated the optimality of root-mean-square (RMS) and mean-absolute-value (MAV) processors for estimating muscle force output [7]. As a result, RMS and MAV signal processors have been extensively emphasized and utilized due to their practicality and effectiveness, especially in direct model-based control of prosthetic systems [8]–[12]. These same sEMG signal features have also been quantitatively evaluated to be some of the most meaningful features when estimating neural activities [13], [14].

However, Windrich et al. highlighted the relatively greater number of studies focused on neural control of upper limb prostheses using sEMG signals compared to studies involving lower-extremity (LE) prostheses [15]. Indeed, there exist unique considerations for LE prostheses, including limited options for sEMG electrode interfacing and significant dynamic pressure changes on the residual limb that can cause structural deformation and electrode contact variation.

In order to overcome these challenges, many studies have presented solutions within various electrical and mechanical engineering domains [16]–[19].

In the signal processing domain, one of the dominant challenges in LE prosthesis applications is mitigating sEMG impulse artifacts produced during ambulatory activities. Specifically, impulsive acceleration at heel-strike can generate drastic pressure changes at the skin-electrode interface as well as vibration in the mechanical connections of the sEMG platform. While De Luca et al. set an effective standard for filtering generic motion artifacts and baseline noise with band-pass filtering, this standard does not consider and handle impulse artifacts [20], [21]. Interestingly, a few bio-signal denoising algorithms that suppress impulse artifacts have been developed within the domain of ECG artifact filtering. These algorithms, including Wavelet analysis, independent component analysis, empirical mode decomposition, and adaptive thresholding, are both insightful and easily applied. Nonetheless, due to these algorithms having been developed for filtering ECG signals, they are potentially unsuitable as real-time impulse artifact filters since they require multiple sEMG channels, demanding high computational costs, and require thorough a-priori knowledge of artifact type [22], [23].

Therefore, in this paper, we present an effective sEMG signal processing method and algorithm for filtering impulse artifacts in extracting time-domain sEMG signal features, such as RMS or MAV. Based upon a probabilistic understanding of recorded sEMG signals and impulse artifact noise, the proposed algorithm leverages real-time cumulative histogram filtering with minimal computational demands. Individual performances of the proposed filtering methods are evaluated on both synthetic sEMG data and real sEMG data collected during use of a transtibial (TT) prosthestic device.

The paper is organized as follows: Section II explains sEMG signal models with impulse artifact models. Section III describes the detailed algorithm for cumulative histogram filtering. Section IV demonstrates and evaluates the proposed filtering algorithm. Finally, Section V presents the paper's discussion and conclusions.

II. BACKGROUND

A. Probabilistic Model of sEMG Signals

Understanding the nature of sEMG signals is critical to utilizing them as control inputs. Though sEMG signals are naturally non-stationary and stochastic, there have still been

several attempts made to understand and model their behavior [7], [14], [24], [25]. In the course of finding an optimal estimation of instantaneous sEMG amplitude, E. A. Clancy and N. Hogan determined that the amplitude distribution of a band-passed sEMG signal could be described as between those of Gaussian and Laplacian PDFs. Fig. 1, recreated from [7], demonstrates this relationship. Correspondingly, because the RMS of Gaussian PDFs is equivalent to their maximum likelihood amplitude with optimal signal-to-noise ratio (SNR), and because the MAV of Laplacian probability density functions (PDFs) is equivalent to their maximum likelihood amplitude with optimal SNR, the researchers determined that both RMS and MAV could be effectively utilized to estimate the signal power of band-passed sEMG.
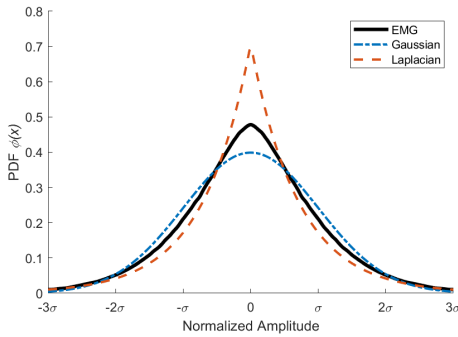

Fig. 1. Normalized experimental probability density estimates of triceps muscle contraction up to 50% maximum voluntary contraction, conducted as experiment II in [7]. Recreated from [7] with permission ©2021 IEEE.

B. Real-time sEMG Feature Extraction

Real-time feature extraction from sEMG follows a typical procedure shared among many related studies [1], [20]. Fig. 2 demonstrates a simplified generic sEMG signal processing pipeline. First, raw sEMG signals are required to be sampled with a frequency of at least 1 kHz to effectively capture the entire signal's power spectrum. Then, sampled raw sEMG signals are processed with a band-pass filter to remove motion artifacts and power-line noise [20], [21]. A moving short-time window with a duration between 100 and 500 milliseconds can then be applied to extract a signal feature at each time step. In cases where normalization of the extracted signal features is required, signal features are divided by the maximum amplitude of those measured at maximum voluntary contraction (MVC). The normalized MAV or RMS features are often utilized as estimates of %MVC to provide a muscle activation ratio (α) for real-time control applications [8]–[12].
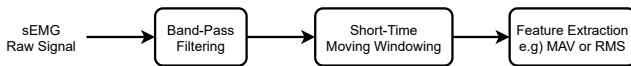

Fig. 2. Generic sEMG signal processing pipeline

C. Modeling Impulse Artifacts

Theoretically, the ideal delta function has unity frequency response along the entire frequency domain, a characteristic that renders band-pass filtering ineffective. When processed by the sEMG processing pipeline shown in Fig. 2, a distinct impulse artifact is produced. As a demonstration, we modeled an impulse as a unipolar sinusoidal signal with unit amplitude and 10 ms duration, as shown in Fig. 3. We then processed the sEMG using the pipeline shown in Fig. 2. The selected band-pass filter was designed as an FIR filter with a pass-band between 20 and 340 Hz and a stop-band attenuation of 80 dB. A short-time window with 200 ms duration was used to extract MAV and RMS features.
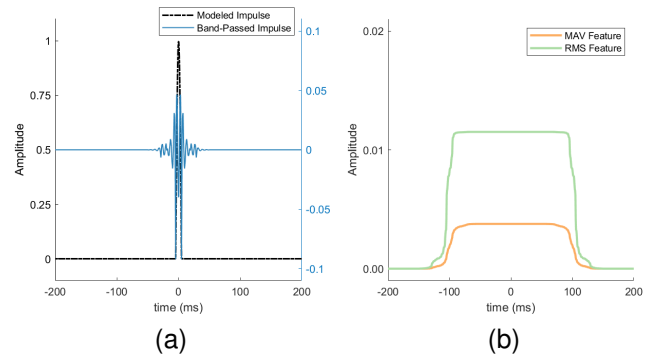

Fig. 3. Modeled impulse signal, its response after band-pass filtering, and corresponding features extracted. The impulse signal is modeled with unit amplitude and 10 ms duration. Peak of impulse onset occurs at 0 s. The response shown is derived in a non-causal manner with zero phase and group delay.

After band-pass filtering, an impulse artifact presented itself in the form of a sinc signal with duration of around 60 milliseconds, approximately three times longer than that of the original peak (when counting up to the third dominant peak). MAV and RMS feature extraction processes on the band-passed artifact signal generated flat output features with amplitude around only 1% of the raw signal amplitude. However, in a situation where the impulse artifact has an order-of-magnitude larger amplitude than the original sEMG signal, it can clearly be seen how the artifact can significantly alter the results compared to processing the sEMG signal alone.

III. METHODS

In this section, we present a cumulative histogram filtering (CHF) algorithm for impulse artifact reduction.

A. Cumulative Histogram Filtering

Fig. 4 introduces the proposed CHF to the generic sEMG processing pipeline from Fig. 2. Within the process demonstrated by Fig. 4, band-passed sEMG signals are sampled using a given time window for every computational time-step in the same way as the generic filtering scheme. However, the proposed CHF processes sEMG data in between the short-time signal windowing and feature extraction steps.
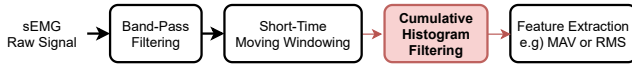
Fig. 4. Modified sEMG signal processing pipeline with the proposed CHF filtering method.

Algorithm 1 describes the CHF process in detail. Fig. 5 visualizes Algorithm 1 in sequential order.

Algorithm 1: Cumulative Histogram Filtering

Data Input : Short-time windowed sEMG data $\mathbf{X}$
Coefficients : Histogram lower bound hLB
              Histogram upper bound hUB
Data Output : Filtered sEMG data $\mathbf{Y}$

1 **begin**
2    $\mathbf{X_{ABS}} \leftarrow abs(\mathbf{X})$;
3    $\mathbf{H} \leftarrow cumulativeHistogram(\mathbf{X_{ABS}})$;
4    $xLB \leftarrow x \in \mathbf{X_{ABS}}$ s.t. $\mathbf{H}[x] = hLB$;
5    $xUB \leftarrow x \in \mathbf{X_{ABS}}$ s.t. $\mathbf{H}[x] = hUB$;
6    $\mathbf{Y} \leftarrow \{x \in \mathbf{X_{ABS}} \mid xLB \leq x \leq xUB\}$
7 **end**

The CHF is conducted over all sampled sEMG signals within the time window. First, samples are sorted by amplitude to generate a cumulative histogram. Then, data samples within a specified continuous range of the histogram are utilized for subsequent feature extraction.

Given the example sEMG dataset shown in Fig. 5a, Fig. 5b shows its histogram and cumulative histogram and Fig. 5c shows the filtered subset of the short-time windowed sEMG samples to be used in feature extraction.

The proposed CHF method is only applicable for certain types of time-domain sEMG signal features. The types of sEMG features compatible with CHF include MAV, RMS, variance (VAR), log-detector, temporal moment (TM), and v-Order processors [26]. These signal features share a common characteristic, namely that the extracted signal features are correlated to overall signal power and energy of sampled sEMG data without considering sEMG signal dynamics. Because the CHF rearranges the signal with no regard to sampling order, time-domain sEMG feature extraction methods that depend on signal dynamics, such as Bayesian filtering, are not compatible with the proposed method.

B. Implementation of the CHF

1) Basic Implementation: While Algorithm 1 demonstrates the procedure of CHF in sequence, Algorithm 2 summarizes an intuitive implementation of the proposed CHF algorithm, as direct implementation of Algorithm 1 in real-time would inefficiently utilize memory space and processing power.
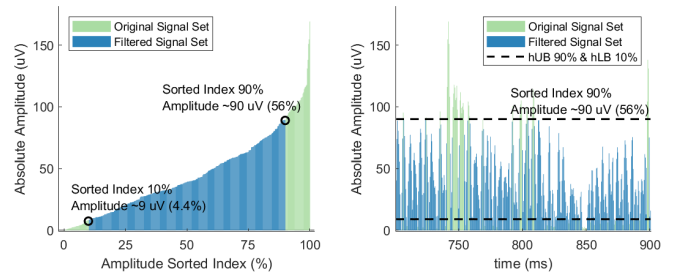
Computation routines in Algorithm 1 (computing cumulative histogram, finding lower and upper bound coefficients, and conditional signal extractions) are implemented in Algorithm 2 by sorting absolute sEMG data by amplitude
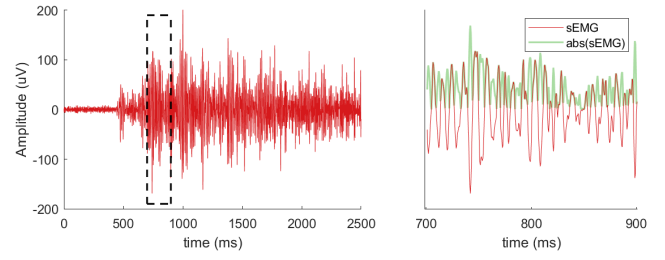
(a)
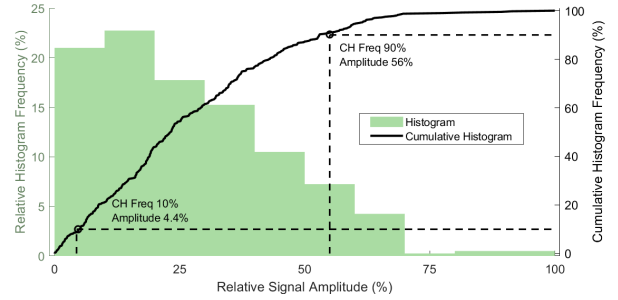
(b)

(c)

Fig. 5. Graphic demonstration of Algorithm 1 and Algorithm 2 with filter coefficients hLB of 10% and hUB of 90%. (a) Example sEMG time series highlighting the short-time windowed signal for feature extraction (b) Histogram plot and cumulative histogram plot extracted from Fig. 5a. The filter coefficients, hLB and hUB, are highlighted with corresponding xLB of 4.4% and xUB of 56%. The distribution of relative amplitudes is observed to be skewed right. (c) Sorted and unsorted sEMG data based on Fig. 5a highlighting original data and filtered data with hLB, hUB, xLB, xUB indicated.

Algorithm 2: Intuitive Implementation of CHF

Data Input : Short-time windowed sEMG data $\mathbf{X}$
Coefficients : Histogram lower bound hLB
              Histogram upper bound hUB
Data Output : Filtered sEMG data $\mathbf{Y}$

1 **begin**
2    $\mathbf{X_{ABS}} = abs(\mathbf{X})$;
3    $\mathbf{S} \leftarrow sort(\mathbf{X_{ABS}})$;
4    $\mathbf{Y} \leftarrow \mathbf{S}[hLB : hUB]$;
5 **end**

---

and indexing a sub-array. The computational complexity of Algorithm 2 is bounded by the computational complexity of the sorting algorithm. Thus, the minimum computational

complexity of Algorithm 2 is $\mathcal{O}(n\log n)$ with fast sorting algorithms such as quick sort that make no assumptions on the underlying data.

2) Real-time Iterative Implementation: The computational complexity of Algorithm 2 can be significantly reduced and optimized by implementing CHF in an iterative scheme. Algorithm 3 provides an iterative CHF implementation.

Algorithm 3: Iterative Implementation of CHF

Update	: Newly sampled sEMG data point x_t
Data Buffer:	$\mathbf{X_{ABS}}$, $\mathbf{S}$
Coefficients :	Histogram lower bound hLB
	Histogram upper bound hUB
Output	: Filtered sEMG data $\mathbf{Y}$

1 **begin**
2   Pop oldest indexed data $x_{ABS,1}$ from Queue $\mathbf{X_{ABS}}$;
3   Remove $x_{ABS,1}$ from Vector $\mathbf{S}$;
4   Push $abs(x_t)$ in Queue $\mathbf{X_{ABS}}$;
5   Insert $abs(x_t)$ in Vector $\mathbf{S}$ based on amplitude;
6     $\mathbf{Y} \leftarrow \mathbf{S}[hLB : hUB]$;
7 **end**

By inserting only newly sampled data into the running data buffers X_{ABS} and S, the sorting operation from Algorithm 2 is no longer required. Algorithm 3 can be considered to be a linked-list style data buffer update scheme.

With Algorithm 3, computational complexity can be reduced to $\mathcal{O}(n)$ due to only requiring linear array traversals. This scheme can easily be implemented in real-time on microcontrollers or microprocessors used with portable mechatronics systems.

IV. EVALUATION

A. Subject Recruitment and Data Collection

A single subject (43 years old, female) with unilateral transtibial amputation participated in data collection for the evaluation of the proposed CHF method. The subject, a recipient of the novel agonist-antagonist myoneural interface(AMI) amputation surgery, possessed two dynamic AMI pairs (Tibialis Anterior (TA) coupled with Lateral Gastrocnemius (LG) and Tibialis Posterior (TP) coupled with Peroneous Longus (PL)) within her residuum [9]. The subject provided written informed consent through MIT COUHES protocol #1812634918.

In the first experimental session, the subject was asked to voluntarily rotate her phantom limb while seated. Raw sEMG signals from TA and TP muscles were collected while the subject wore her prescribed prosthetic socket and a liner. A custom embedded sEMG acquisition system was utilized along with flexible (sub-liner interface for prosthetic-SLIP) electrodes designed for within-socket sEMG acquisition [16], [27], [28]. Raw sEMG signals were processed with a digital band-pass FIR filter with pass-band of 40 to 340 Hz and stop-band attenuation of 80 dB. A short-time window with duration of 200 ms was used for subsequent CHF processing.

Fig. 6 shows the collected reference data processed using the generic technique illustrated in Fig. 2 to yield RMS and MAV features. In a second experimental session, sEMG data were acquired during ambulatory activity to evaluate the efficacy of the proposed CHF scheme illustrated in Fig. 4.
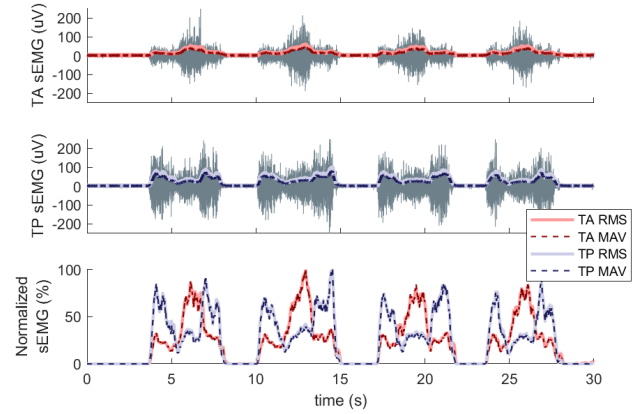

Fig. 6. Reference sEMG data collected from TA and TP muscles during voluntary rotational movement of the residual phantom limb. The plot visualizes both RMS and MAV processing outputs.

For qualitative evaluation of the CHF algorithm in real situation, sEMG data during ambulation were also collected from the identical subject with identical sEMG measurement setup [28]. With a purpose to evaluate an efficacy of CHF algorithm, the flexible SLIP electrodes were placed without conductive gel resulting the system more susceptible to impulsive artifacts during gait.

B. Performance Analysis with Clean sEMG Signals

This subsection utilizes the sEMG data from the first experimental session to quantitatively compare the output of CHF to generic sEMG processing in the absence of impulse artifacts. In general, higher similarity between results is more desirable, implying that the proposed CHF does not suppress or distort original information from the sEMG signals.

Using data shown in Fig. 6, we applied the proposed CHF while sweeping filter coefficient hLB from 0% to 40% and hUB from 60% to 100% with a step size of 2.5%, resulting in 289 sets of cutoff boundaries per channel and processor. We processed sEMG data from the subject's TA and TP muscle channels with MAV and RMS processors, resulting in a total of 1156 processed sEMG time series.

1) Pearson's Correlation: We analyzed Pearson's correlation coefficients to quantify the correlation of the processed sEMG data. Table I shows the result of the correlation analysis.

All of the correlation coefficients from both TA and TP muscles with RMS and MAV processors present mean values greater than 0.99, implying that CHF processed data are highly correlated with unfiltered sEMG data. Because the data from the TP muscle with RMS processor show the lowest minimum correlation values of 0.9837, individual correlation coefficients of these data are partially presented in Table II.

Muscle	Signal Feature	Correlation Coefficients		
		Mean	Variance	Min
Tibialis	RMS	0.9954	5.51e-6	0.9915
Anterior	MAV	0.9983	1.22e-6	0.9959
Tibialis	RMS	0.9925	2.44e-5	0.9837
Posterior	MAV	0.9968	6.08e-6	0.9915

TABLE II

CORRELATIONS OF CHF PROCESSED sEMG SIGNALS:
INDIVIDUAL COEFFICIENTS - TP MUSCLE, RMS PROCESSOR

hLB \ hUB	100%	90%	80%	70%	60%
0%	1.0000	0.9965	0.9924	0.9881	0.9837
10%	1.0000	0.9965	0.9925	0.9881	0.9837
20%	1.0000	0.9965	0.9925	0.9883	0.9839
30%	1.0000	0.9967	0.9928	0.9887	0.9845
40%	0.9999	0.9969	0.9933	0.9894	0.9856

With a minimum observed Pearson's correlation of 0.9837, all of the CHF processed data show high correlation to their original signals. Fig. 7 presents a qualitative comparison of the CHF-processed RMS data from TA and TP muscles.
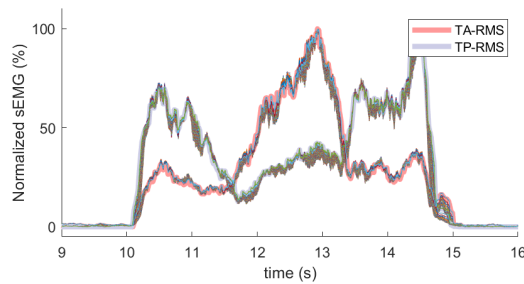

Fig. 7. Partial results from all 289 filtered sEMG series using swept boundary coefficients *hUB* and *hLB* of CHF, processed from the original reference sEMG of Fig. 6. Partial data from 9 to 16 seconds shown.

2) Signal-to-noise Ratio: Signal-to-ambient-Noise-Ratio (SNR) of the CHF processed data are also compared with the SNR of the original data. Ambient noise is defined as the mean value of sEMG data collected and processed during the initial 5 seconds of the trial when the subject was instructed to rest, as shown in Fig. 6. SNR is subsequently defined as the ratio between the maximum measured value and the ambient noise. Fig. 8 shows the result of the SNR analysis.

While the correlational relationship between CHF and SNR is shown to be non-linear, relative SNRs of the data remain higher than 95% compared to the SNRs of unfiltered data in all CHF processed data. Importantly, SNRs of the CHF-processed sEMG data from the TP muscle increase with decreasing *hUB*.

C. Artifact Suppression Performance Analysis

1) Synthetic Impulse Artifact Model: A synthetic sEMG impulse was injected into the data collected from the first session to quantitatively evaluate the CHF's ability to suppress
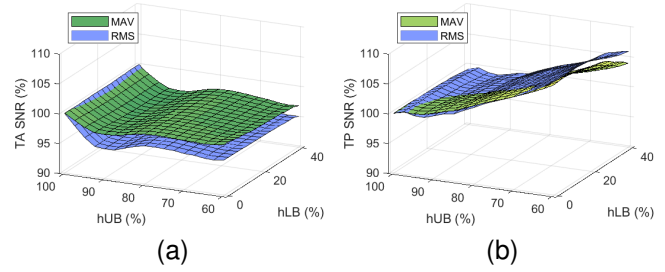

Fig. 8. Effect of filtering on SNR of reference sEMG data from Fig. 6 with swept filter coefficients. (a) Relative SNR of the filtered TA sEMG data. Filtering preserves at least 95% relative SNR for both MAV and RMS features. (b) Relative SNR of the filtered TP sEMG data. As opposed to the TA muscle, filtering of the TP muscle data results in increased SNR.

artifacts. The impulse model from Section II was utilized to synthesize the artifact-affected sEMG dataset. A unipolar impulse with duration of 20 milliseconds and amplitude of 5 mV, approximately 25 times larger than the maximum of band-passed sEMG data was used. A periodic impulse train with impulses every 1 second was generated and added to the raw sEMG data. Fig. 9 shows the synthesized reference data and its simulated signal output with RMS and MAV processors.
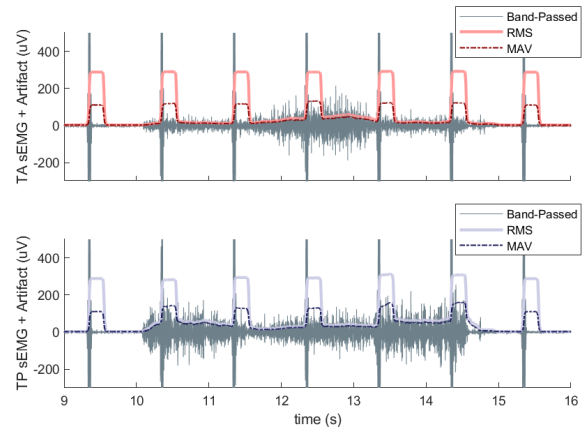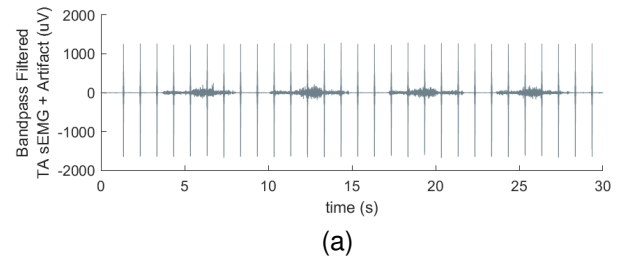

Fig. 9. Synthesized artifact-affected sEMG data. (a) Artifact-affected and band-passed TA muscle sEMG. (b) Effect of impulse artifacts on output RMS and MAV features. Partial data from 9 to 16 seconds are shown.

2) Artifact Suppression Ratio: Artifact suppression ratio is defined as the average ratio of outputs between filtered and non-filtered data sampled at the center of each artifact impulse. The synthesized sEMG data with impulse artifacts

were processed using the CHF filter and swept boundary coefficients in a manner identical to the process of subsection IV-B. Fig. 10 shows the result of the artifact suppression ratio calculation.
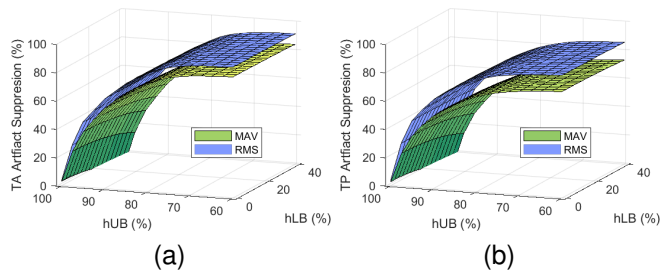

Fig. 10. Artifact suppression ratio analyses with swept *hLB* and *hUB* filter coefficients. Artifact suppression ratio is largely correlated with *hUB*. (a) Artifact suppression ratio of the TA. (b) Artifact suppression ratio of the TP.

From the data, artifact suppression ratio is inversely correlated with *hUB*. Fig. 11 visualizes the effect of varying *hUB* on noise suppression.
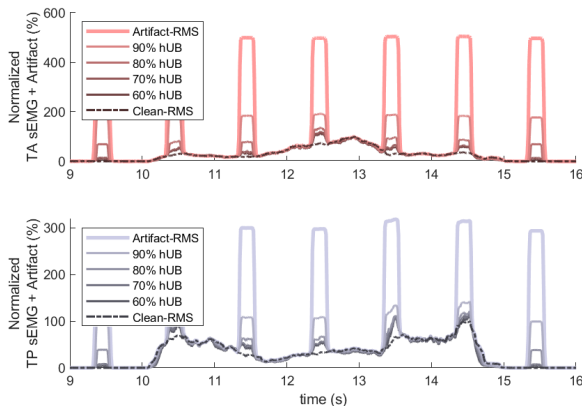

Fig. 11. Synthesized sEMG data shown in Fig. 9 are processed with *hLB* of 10% and *hUB* of 60%, 70%, 80%, and 90%. As *hUB* of CHF algorithm decreases, the corresponding resultant noise from the simulated impulse artifact decreases.

D. Case Study: Ambulation

This subsection presents results from the second experimental session involving ambulatory activity. Fig. 12 shows the sEMG data collected from the TA and TP muscles of the subject's residuum within her socket during ambulation. The collected data are processed using CHF algorithm with hLB of 10% and *hUB* of 60%, 70%, 80%, and 90%. The comparisons of the data processed with and without CHF algorithm were then analyzed.

In Fig. 12, impulse artifacts synchronized with ground reaction force (GRF) peaks are clearly visible in the sEMG data collected from both TA and TP muscles. The results from non-CHF RMS processed sEMG data demonstrate staircase-like plateaus in their output waveforms. With CHF,
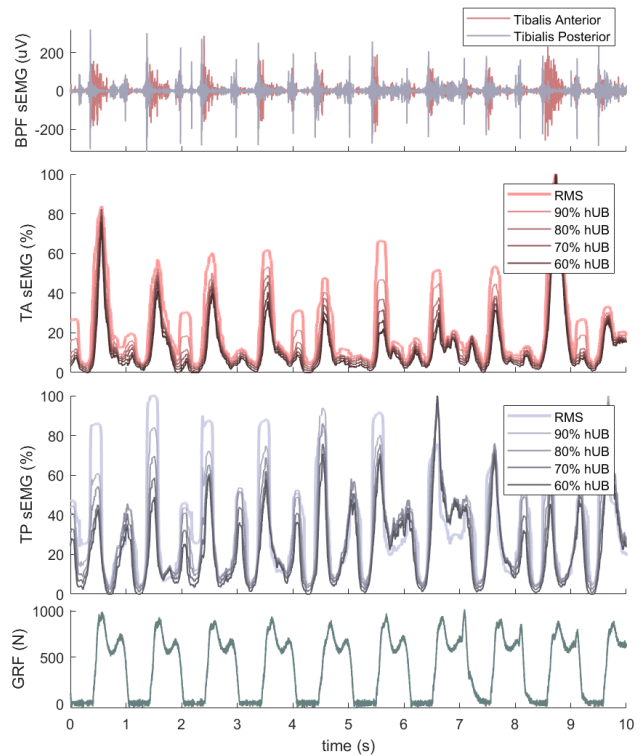

Fig. 12. sEMG data collected during ambulation were processed using CHF algorithm with *hLB* of 10% and *hUB* of 60%, 70%, 80%, and 90% for RMS processing. Impulse artifacts are synchronized with ground reaction force peaks, but suppressed in the resulting RMS signal features as *hUB* decreased.

staircase-like plateaus are suppressed, yielding output waveforms which more qualitatively resemble natural activation patterns. Though there are no ground truth reference labels for sEMG data and impulse artifact sources within the given dataset, we feel the CHF's efficacy are compelling.

V. DISCUSSION

This paper developed a filtering technique capable of robustly extracting time-domain features from sEMG signals in the presence of undesired impulse artifact. The proposed CHF method was shown to effectively filter out synthetic impulse artifacts in a reference sEMG data set while preserving the signals' underlying information.

Intuitively, the CHF method exploits the different PDFs of the sEMG signal and noise models as described in Section II. Because impulse artifacts under the tested conditions demonstrated a right-skewed PDF compared to the underlying sEMG's PDF, the CHF algorithm effectively filters the artifacts out by discriminating via signal amplitude. The CHF method is able to leverage a limited range of information from the middle portion of a time window's cumulative distribution, and as seen in Fig. 11, this omission of high-amplitude samples enabled extraction of sEMG features with comparable levels of SNR compared to an artifact-free reference data set.

At the extreme limit, the CHF method becomes identical to the median feature extraction method with *hLB* and *hUB*

at 50%. Admittedly, the optimality of the median processor as a muscle force estimator has not been compared to MAV or RMS processors. However, due to the stochastic nature of sEMG, features that utilize multiple samples when extracting information from an sEMG signal may vary less compared to the one produced by the median processor which depends on a single median sample. As CHF-filtered MAV and RMS features with reasonable *hLB* and *hUB* ranges demonstrated high correlations to non-filtered MAV and RMS features, it is suggested that the proposed CHF method does not disrupt the optimal nature of the MAV and RMS features discussed in Section II.

Though this preliminary study yielded promising results, the proposed filtering method remains to be tested thoroughly with more data collected under additional testing conditions. Future work will investigate the formulation of a data-driven optimization scheme to determine CHF coefficients *hUB* and *hLB* based on an underlying sEMG reference data set. As it is, the proposed CHF method is efficiently computed with minimal latency from input to output, and the authors hope that this work will assist research efforts toward real-time control of robotic mechatronics using sEMG signals under dynamic conditions.

ACKNOWLEDGMENT

REFERENCES

[1] D. Farina, R. Merletti, and R. M. Enoka. The extraction of neural strategies from the surface EMG: an update. *Journal of Applied Physiology*, 117(11):1215–1230, 2014.

[2] C. J. De Luca. The use of surface electromyography in biomechanics. *Journal of applied biomechanics*, 13(2):135–163, 1997.

[3] Dario Farina, Roberto Merletti, and Roger M Enoka. The extraction of neural strategies from the surface EMG. *Journal of applied physiology*, 96(4):1486–1495, 2004.

[4] Neville Hogan and Robert W Mann. Myoelectric signal processing: Optimal estimation applied to electromyography-part i: Derivation of the optimal myoprocessor. *IEEE Transactions on Biomedical Engineering*, (7):382–395, 1980.

[5] Mark Ison and Panagiotis Artemiadis. The role of muscle synergies in myoelectric control: trends and challenges for simultaneous multi-function control. *Journal of neural engineering*, 11(5):051001, 2014.

[6] Neville Hogan and Robert W Mann. Myoelectric signal processing: Optimal estimation applied to electromyography-part ii: experimental demonstration of optimal myoprocessor performance. *IEEE Transactions on biomedical Engineering*, (7):396–410, 1980.

[7] Edward A Clancy and Neville Hogan. Probability density of the surface electromyogram and its relation to amplitude detectors. *IEEE Transactions on Biomedical Engineering*, 46(6):730–739, 1999.

[8] Samuel K Au, Paolo Bonato, and Hugh Herr. An emg-position controlled system for an active ankle-foot prosthesis: an initial experimental study. In *9th International Conference on Rehabilitation Robotics, 2005. ICORR 2005.*, pages 375–379. IEEE, 2005.

[9] T. R. Clites, M. J. Carty, J. B. Ullauri, M. E. Carney, L. M. Mooney, J. F. Duval, S. S. Srinivasan, and H. M. Herr. Proprioception from a neurally controlled lower-extremity prosthesis. *Science Translational Medicine*, 10(443):1–13, may 2018.

[10] Carl D Hoover, George D Fulk, and Kevin B Fite. The design and initial experimental validation of an active myoelectric transfemoral prosthesis. *Journal of Medical Devices*, 6(1), 2012.

[11] Carl D Hoover and Kevin B Fite. A configuration dependent muscle model for the myoelectric control of a transfemoral prosthesis. In *2011 IEEE International Conference on Rehabilitation Robotics*, pages 1–6. IEEE, 2011.

[12] Sophie M Wurth and Levi J Hargrove. Real-time comparison of conventional direct control and pattern recognition myoelectric control in a two-dimensional fitts' law style test. In *2013 35th Annual International Conference of the IEEE Engineering in Medicine and Biology Society (EMBC)*, pages 3630–3633. IEEE, 2013.

[13] Angkoon Phinyomark, Franck Quaine, Sylvie Charbonnier, Christine Serviere, Franck Tarpin-Bernard, and Yann Laurillau. Emg feature evaluation for improving myoelectric pattern recognition robustness. *Expert Systems with applications*, 40(12):4832–4840, 2013.

[14] Angkoon Phinyomark, Rami N Khushaba, and Erik Scheme. Feature extraction and selection for myoelectric control based on wearable emg sensors. *Sensors*, 18(5):1615, 2018.

[15] Michael Windrich, Martin Grimmer, Oliver Christ, Stephan Rinderknecht, and Philipp Beckerle. Active lower limb prosthetics: a systematic review of design issues and solutions. *Biomedical engineering online*, 15(3):5–19, 2016.

[16] Seong Ho Yeon, Tony Shu, Emily A Rogers, Hyungeun Song, Tsung-Han Hsieh, Lisa E Freed, and Hugh M Herr. Flexible dry electrodes for emg acquisition within lower extremity prosthetic sockets. In *2020 8th IEEE RAS/EMBS International Conference for Biomedical Robotics and Biomechatronics (BioRob)*, pages 1088–1095. IEEE.

[17] H. Posada-Quintero, R. Rood, K. Burnham, J. Pennace, and K. Chon. Assessment of carbon/salt/adhesive electrodes for surface electromyography measurements. *IEEE J Transl Eng Health Med*, 4(2100209), 2016.

[18] AJ Young, TA Kuiken, and LJ Hargrove. Analysis of using emg and mechanical sensors to enhance intent recognition in powered lower limb prostheses. *Journal of neural engineering*, 11(5):056021, 2014.

[19] Stephanie Huang. *Continuous Proportional Myoelectric Control of an Experimental Powered Lower Limb Prosthesis During Walking Using Residual Muscles.* PhD thesis, 2014.

[20] Carlo J De Luca, L Donald Gilmore, Mikhail Kuznetsov, and Serge H Roy. Filtering the surface emg signal: Movement artifact and baseline noise contamination. *Journal of biomechanics*, 43(8):1573–1579, 2010.

[21] Bernabe Rodríguez-Tapia, Israel Soto, Daniela M Martínez, and Norma Candolfi Arballo. Myoelectric interfaces and related applications: Current state of emg signal processing–a systematic review. *IEEE Access*, 8:7792–7805, 2020.

[22] Sara Abbaspour, Maria Lindén, and Hamid Gholamhosseini. Ecg artifact removal from surface emg signal using an automated method based on wavelet-ica. In *pHealth*, pages 91–97, 2015.

[23] Ping Zhou, Blair Lock, and Todd A Kuiken. Real time ecg artifact removal for myoelectric prosthesis control. *Physiological measurement*, 28(4):397, 2007.

[24] IW Hunter, RE Kearney, and LA Jones. Estimation of the conduction velocity of muscle action potentials using phase and impulse response function techniques. *Medical and Biological Engineering and Computing*, 25(2):121–126, 1987.

[25] Edward A Clancy, Evelyn L Morin, and Roberto Merletti. Sampling, noise-reduction and amplitude estimation issues in surface electromyography. *Journal of electromyography and kinesiology*, 12(1):1–16, 2002.

[26] Mahyar Zardoshti-Kermani, Bruce C Wheeler, Kambiz Badie, and Reza M Hashemi. Emg feature evaluation for movement control of upper extremity prostheses. *IEEE Transactions on Rehabilitation Engineering*, 3(4):324–333, 1995.

[27] S. H. Yeon. Design of an advanced sEMG processor for wearable robotics applications. Master's thesis, Massachusetts Institute of Technology, 2019.

[28] Seong Ho Yeon, Tony Shu, Hyungeun Song, Tsung-Han Hsieh, Junqing Qiao, Emily A Rogers, Samantha Gutierrez-Arango, Erica Israel, Lisa E Freed, and Hugh M Herr. Acquisition of surface emg using flexible and low-profile electrodes for lower extremity neuroprosthetic control. *IEEE Transactions on Medical Robotics and Bionics*, 2021.